EasyChair Preprint

№ 1808

Prototype Loading Tests on the Mechanical behaviors of the Shield Lining Structure of a Water Storage and Sewage Tunnel

Yeting Zhu, Yanfei Zhu, Qi Wang, Zixin Zhang, Xin Huang and Wei Liu

October 31, 2019

Prototype Loading Tests on the Mechanical behaviors of the Shield Lining Structure of a Water Storage and Sewage Tunnel

ZHU Yeting[1], ZHU Yanfei[1], WANG Qi[1], ZHANG Zixin[2], HUANG Xin[2], LIU Wei[2]

[1]*Shanghai Tunnel Engineering Co. Ltd., Shanghai 200233, China*

[2]*Department of Geotechnical Engineering, Tongji University, Shanghai 200092, China*

Email: 1210278theronzhu@tongji.edu.cn

ABSTRACT: A sophisticated and flexible testing system that can simulate both external water-soil pressures and inner water pressure was designed, based on which both single-ring and three-ring full-scale loading tests were conducted, and some interesting observations were made: increasing inner water head decreased the axial force, which thereby increased the lining deformation; the bending moment transferring mechanism was evident in the three-ring tests due to staggered fabrication, which significantly reduced the structural deformation comparing with the single-ring tests; the structural deformation accumulated slightly during the water inflow and drainage cycles, and the structural deformations remained stable after nine loading cycles; the internal forces increased and convergence deformations decreased as hoop effect was caused by the uniformly distributed grouting pressures; increasing longitudinal thrust made the 3D effects more obvious but the influence of increasing longitudinal thrust was limited as the structural deformation became approximately saturated when the longitudinal thrust exceeded a certain threshold value; compared with the increasing of the buried depth, the sensitivity of the lining deformation to the coefficients of subgrade reaction was more obvious during the increasing of the inner water head, and the deformation values at the UST state decreased linearly with the coefficients; both the cracking process captured by DIC technique and measured overall deformations showed that the lining structure failed when the inner water head exceeded 65m (ultimate limit states) .

KEYWORDS: Shield tunnel; Mechanical behavior; Loading test; Inner water head; Strata resistance

1 Introduction

Shield tunneling, which is a fully-mechanized construction method with sufficient safety during excavation and lining work, has a number of merits, such as small disturbance to ground traffic or river navigation, and little vulnerability to climatic conditions. The aforementioned merits make the shield tunneling the most widely used tunnel construction method, especially in the urban core districts where main political, economic, cultural activities are concentrated and substantial underground facilities congest (Liu et al., 2014; Selemetas et al., 2014; Gragnano et al., 2015; Zhang et al., 2016).

Shield lining system, a longitudinally fabricated cylinder structure, is composed of a certain number of individual segments fabricated through different types of bolts. The mechanical responses of such a structure are complex and can be influenced by many factors. Normally, when designing a lining system, the lining structure is simplified as a homogenous structure. Recent studies have shown that 2D homogeneous ring model could not really and fully reflect the influence of the joints (Lee & Ge, 2001; Teachavorasinskun & Chub-Uppakarn, 2010), staggered-jointed assembling effect (Arnau & Molins, 2011) and the interaction between the lining rings (Zhang et al., 2017). Therefore, 3D analyses including scaled model tests, prototype loading tests, numerical simulation were adopted frequently to explore the three-dimensional mechanical responses when the shield linings were subjected to the soil and water pressures. Among them, the full-ring prototype loading tests were considered to be the most reliable approach as it does not have the scaled effect, can realize the mechanical integrity and simulate the real assembling and loading conditions. Furthermore, it is also more versatile, repeatable and flexible compared with field in-situ tests. Therefore, full-ring loading tests on the mechanical behaviors and damage modes of the linings were frequently conducted before the constructions of a new project, especially when special and complex hydrogeological conditions were involved (Molins & Arnau, 2011; Afshan et al., 2017; Huang et al., 2018) or new lining cross-section was adopted (Nakamura et al., 2003; Liu et al., 2018; Zhu et al., 2018; Zhang et al., 2019).

In recent years, urban heat island effect and rain island effect intensify the frequency of extreme weather such as heavy storms. Ground surface hardening coverage rate is increasing while the seepage capacity of the surface decreases rapidly. Thus, ‘sponge city’ was firstly proposed in 2012 to avoid flooding and collects rainwater effectively in China, and the deeply-buried water storage and drainage tunnels (WSD tunnel) are the main collectors to swallow and spit the rainwater and sewage. Shanghai, the economic center of China, started a ‘Deep Shield Tunnel’ project beneath Suzhou River in 2016 to improve the drainage standards and the ability to deal with heavy storms of the area along the river. However, several issues have to be faced during the design of the shield lining. Firstly, almost all newly planned or constructed WSD tunnels are located between 50 m and 100 m beneath the ground surface. Due to the very soft nature and high sensitivity of soil formations, the full-cover soil depth has to been considered, which leads to high design load of soil and water pressure on the lining structure. Secondly, unlike normal transportation and utility tunnel, WSD tunnels experience inner hydrostatic pressures during heavy storms besides normal external water and soil pressures. The structural response and mechanical behaviors of the lining structure subjected to inner water pressure are not clear. Thirdly, the WSD tunnels will experience repeating water inflow and drainage cycles during service period, the long-term structural stability of the lining system under the alternating loads is difficult to be determined.

In this paper, single-ring and three-ring prototype loading teste were employed to assess the stability and reliability of the designed segmental lining and explore the mechanical behaviors of the lining structure under 2D (a full ring) and 3D (a full ring and two half rings) assembling conditions. The influences of the inner water head on the mechanical response of the segmental lining were investigated. The effect of staggered fabrication was revealed through the comparisons between the data of single-ring and three-ring tests. Furthermore, the mechanical behavior of the lining structure subjected to repeating changes of inner water head was also explored. In addition, some sensitivity analyses were also conducted to investigate the influences of some key construction parameters on the structural responses of the water storage and sewage tunnel. Finally, the damage modes of the lining structure were discovered.

2 Project Background

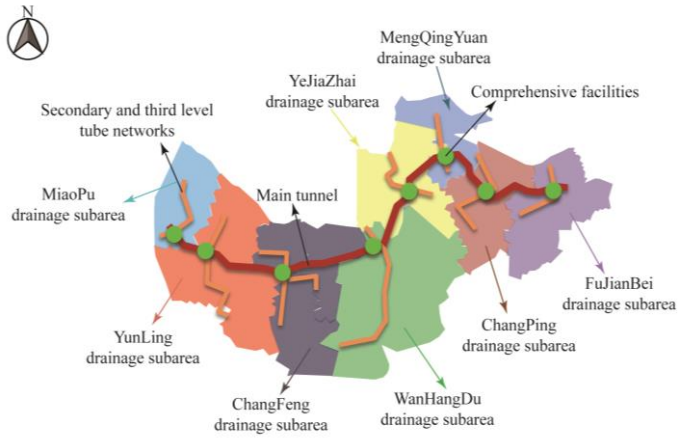

Figure 1 Route of the main tunnel and eight drainage subareas

As shown in Figure 1, according to the plan of Shanghai government (Huang et al., 2019), an ultra-deep water storage and drainage pipeline system will be built to serve 25 drainage systems located at Changning, Pudong, Jing'an and Huangpu districts along the Suzhou River, which consists of a main tunnel, 8 comprehensive facilities, secondary and third tube networks (divided into 8 subareas). The total service area will be 57.9 km^2. It is planned for regulating the peak rainfall which will be conveyed pretreated before discharging into Suzhou River. Once this project has been completed, the core functions of drainage and waterlogging prevention, and initial rain management can be realized, which thereby will upgrade the existing water storage and sewage system and further enrich the water control methods.

The main tunnel has a total length of 15.3km stretching from MiaoPu Greenland in the west to Fujian North pump station in the east, which is located between 40 m to 50 m beneath the Suzhou River. According to the original design plan, the main tunnel, with an inner diameter of 9 m, has a total volume of about 1 million cubic meters, equivalent to 400 standard swimming pools.

3 Testing segment

The designed buried depth of the tunnel crown was finally determined to be 50m, and the underwater table was considered to be 48m above the tunnel crown. The detailed illustration of the geological condition, the design loads, segmental layout and joint configuration are shown in Figure 2.

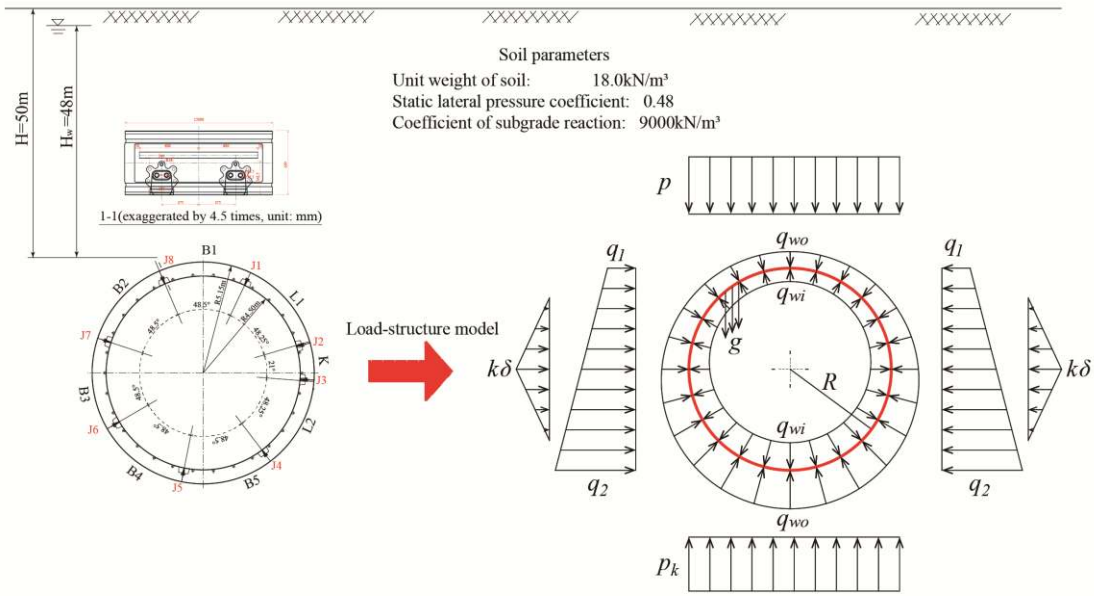

Figure 2 Design consideration and layout of the lining segments

A load-structure model was adopted. Apart from the loads considered for the design of conventional transportation and utility tunnels, including the structural self-weight (g), the overburden pressure (p), the lateral earth pressure varying linearly from q_1 (crown) to q_2 (invert), the external water pressure (q_{wo}), the subgrade reaction pressure (p_k) and the classic triangular lateral resistance pressure presented in the area 45 degrees above and below the horizontal symmetry axis, the inner water pressure (q_{wi}) was also considered.

The lining segment was 0.65 m thick and had a ring width of 1.5 m. The segments cast by CF60 steel fiber reinforced concrete were fabricated by the staggered joint assembling method. Each lining ring consisted of eight blocks, including one key block (F), two adjacent blocks (L1 and L2) and five standard blocks (B1~B5), which were hinged circumferentially by four M36 straight bolts. The neighboring rings were connected by 30 M30 tilting bolts in the longitudinal direction.

Seen from Figure 3, an isolated ring was adopted in the single ring tests, and the three-ring structure consisted of an upper half ring, a middle full ring and a bottom half ring. To simulate the staggered fabrication between neighboring rings, the middle full ring was twisted for 24°. This is the smallest unit representing the staggered fabrication pattern.

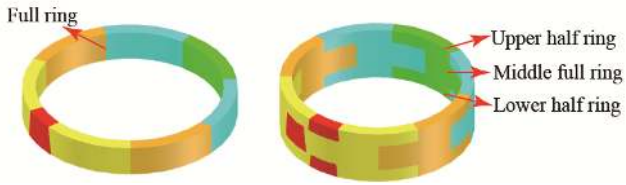

(a)Single ring (b)Three rings

Figure 3 Lining systems for single-ring and three-ring tests

4 Prototype loading test setup

4.1 Loading configuration

Due to the large burial depth and the presence of inner water pressure, a new loading system was developed, which was composed of an external pushing system and an inner pulling system. Specifically, the former contained 15 pairs of loading points (P1 to P15) axisymmetric with respect to the middle central axis. The external loads shown in Figure 2 can be applied through hydraulic jacks installed at these pairs of loading points. The latter was composed of 15 loading points which were evenly distributed over the periphery of the testing segments. Identical loads were applied at these loading points through hydraulic jacks by C-shape steel beams connected to the middle steel column through radial pulling rods to simulate the isotropic water pressure.

Several advantages could be figured out from this new loading method. Unlike the existing centrosymmetric loading method (Liu et al., 2016), the axisymmetric loading configuration could simulate the more realistic distribution mode of the strata pressure as shown in Figure 2. The loading system was divided into one axis-symmetric part and one isotropic part, which worked independently. Such a configuration separated the applications of external soil-water pressures and inner water pressure, which eased the simulation of the influence of the inner water head. Another merit of such a configuration was that the total steel consumption decreased as the loads that originally sustained by a single loading frame were distributed to two loading frames. The whole loading frame had an external dimension of 13.7m×13.7m×4.8m with a total weight of 200 tons (see Figure 4). It lied on the steel ball bearing plates to mitigate the basal friction between the testing specimens and the ground.

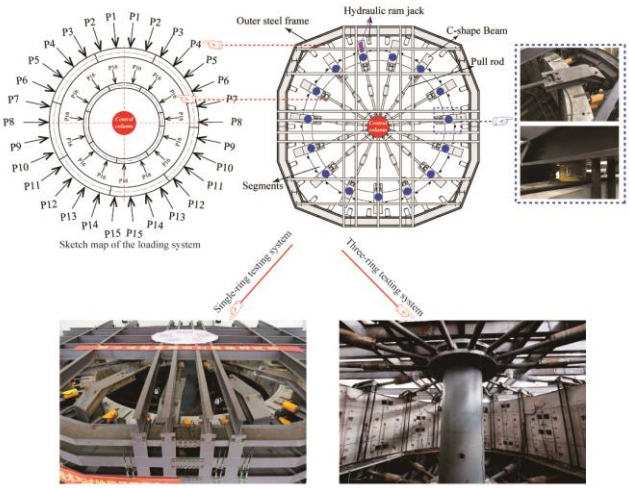

Figure 4 Layout of the loading system

For the external pushing loading system, two hydraulic jacks were used in each external loading points of the full ring in the single-ring tests, and an additional hydraulic jack was set up at each loading point of each half ring in the three-ring tests. Distributing steel beams were installed at the heads of the hydraulic jacks to avoid stress concentration. The hydraulic jacks at each pair of loading points were controlled by one valve, and 15 valve blocks were employed to apply the different soil loads.

For the inner pulling loading system, eight hydraulic jacks were fixed on each C-shape beam, among them, four were on the full ring in the single-ring tests, and two on each half ring in the three-ring tests. All the hydraulic jacks were controlled by only one valve block to provide the same water loads.

To investigate the influence of longitudinal thrust, during the three rings tests, another set of hydraulic jacks (15 in total) was placed between the segments and each C-shape beam to provide the longitudinal thrust forces through two longitudinal pull rods located at the openings of C-shape beam (see Figure 4).

Assembling of such a 'giant' loading system is challenging and time-consuming. The assembling process of the loading frame and the segments for the single-ring tests is shown in Figure 5. In order to ensure the assembling accuracy and efficiency, all components were prefabricated and then transported to the testing site. The installation process was briefed as following:

- Step 1: the steel ribs of the bottom frame were welded and hoisted to the designated location (Figure 5a);
- Step 2: the circumferential backup frame including four π members and four connecting blocks was assembled by bolts and was welded to the bottom frame (Figure 5b);
- Step 3: 15 pairs of jacks (P1~P15) were fixed on the outer frame, and cushion blocks with different sizes were used between the jacks and the frame to adjust the loading angle (Figure 5c);
- Step 4: the jacks were inserted into the groove of the C-shape beams (Figure 5d);
- Step 5: C-shape beams were hoisted and connected to the central column through the pull at the bottom (Figure 5e);
- Step 6: the steel ball bearing plates were laid on the bearings to support the segments (Figure 5f);
- Step 7: segments were fabricated (Figure 5g);
- Step 8: the top pulling rods of the C-shape beams and the outer frame were installed (Figure 5h).

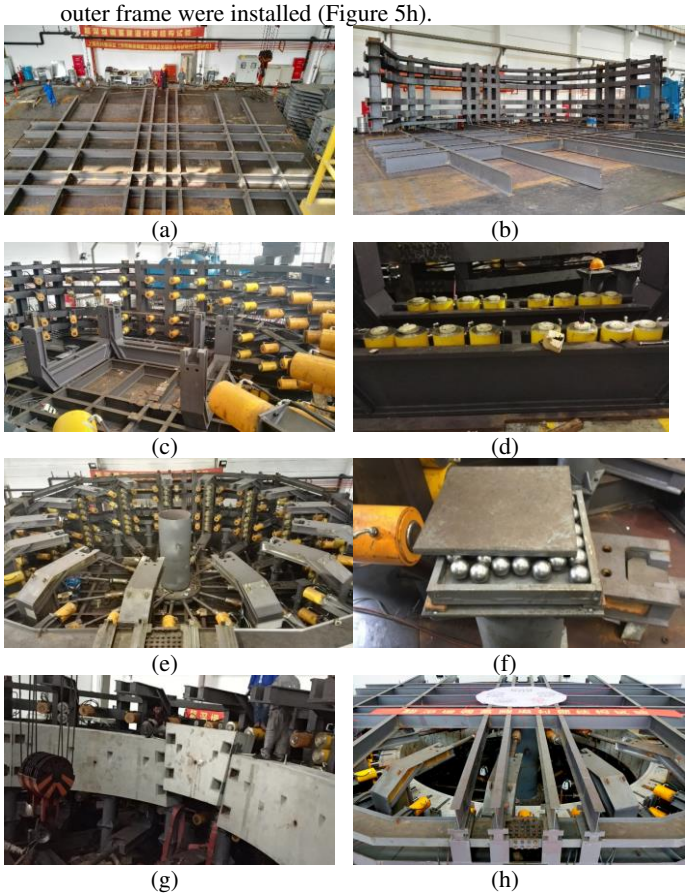

Figure 5 Assembly process of the loading frame and the segments in the single-ring loading tests.

4.2 Loading scheme

As shown in Figure 6, four loading scenarios were considered to explore the mechanical behavior during both construction and service periods, and to determine the bearing capacity and failure mode of the lining structure, including a designed condition, a

cyclic loading condition, a grouting condition and an ultimate loading condition. Among them, the designed condition was the benchmark which involved the following five steps:

Step 1: the buried depth of the tunnel increased from 0m to the designed depth of 50m without water inflow (ET state);

Step 2: the burial depth remained unchanged but the inner water head increased gradually from empty tunnel (ET) to semi-tunnel state (ST) and then to full tunnel state (FT). This loading step simulated the normal working state when the flood was small;

Step 3: the inner water head increases further from FT state to UST state in which the inner water reached the ground surface (50 m taking the tunnel crown as the reference). This simulated the most adverse service condition in which the rainfall was extremely heavy and poured down at a very short period;

Step 4: Drainage stage, the inner water head decreased to the empty tunnel state;

Step 5: Unloading stage, the buried depth decreased to 0m.

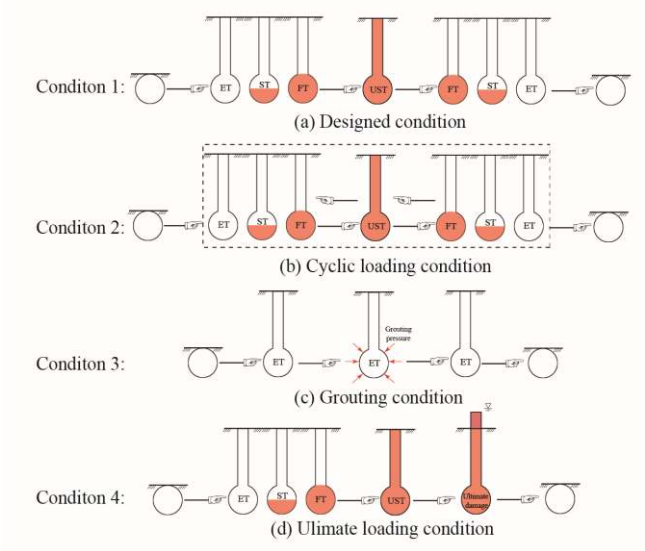

Figure 6 Four loading conditions

The applied hydraulic jack forces during the loading and unloading process of the designed condition in the single-ring tests were shown in Figure 7.

In the cyclic loading condition, step 2 to step 4 were repeated for several times to simulate the water storage and drainage process, which evaluated the working performance and the structural stability of the WSD tunnel in the service life. In the grouting loading case, three pairs of grouting pressures were applied by changing the hydraulic jack forces at corresponding grouting locations. Eventually, to determine the largest inner water pressure that the lining segments can sustained and to identify the failure mode and cracking pattern, the inner water head was increased continuously until the lining structure failed. This was different from traditional bearing capacity loading tests which was achieved by increasing the external soil-water pressures.

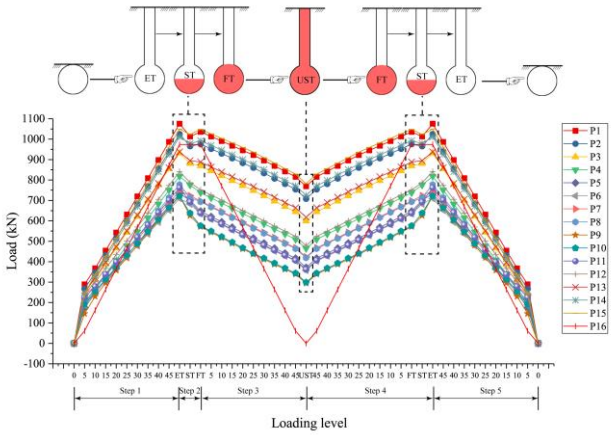

Figure 7 Loading path of the designed loads

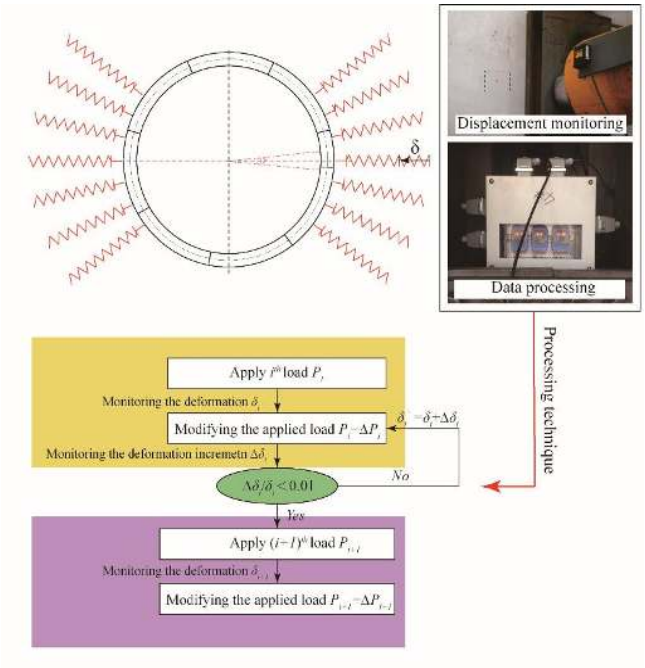

Figure 8 Adaptive strata resistance system

During the three-ring loading tests, a novel 'soil spring' loading system (Figure 8) was developed to simulate the soil-structure interaction in the waist area. Unlike the conventional full-scale loading tests and that prescribed in the design code which consider the lateral soil resistance as a constant, the lateral soil resistance varied with respect to the lining deformation based on Winkler model (Bowles, 1988) determined by Eq. 1. Four laser displacement sensors were installed on the outer steel frame at the loading points from P5 to P11 where the traditional classic resistance existed to measure the deformation of lining structure. When the i^{th} soil and water loads (P_i) were applied on the lining system, the average value of four sensors δ_i at each loading point was acquired and calculated through the acquisition instrument after the segments deformed, then the corresponding adaptive lateral resistance pressure ΔP_i was calculated as:

$$\Delta P_i = k\delta_i \cdot A = k\delta_i \cdot R\theta b \quad (1)$$

where k was the coefficient of subgrade reaction, R was the external diameter of the lining, b stands for the width of the segment, and $\theta = 12°$ is the central angle between two adjacent loading points. ΔP_i was superimposed into the P_i to simulate the soil-structure interaction. If the deformation increment $\Delta\delta_i$ was smaller than 0.01 δ_i, the (i+1)th loads would be applied; otherwise,

$\Delta\delta_i$ was superimposed on the δ_i to modify the ΔP_i until the $\Delta\delta_i/\delta_i < 0.01$.

The loading schemes of the three-ring loading tests were shown in Table 1. Among them, No.1 and No.2 were used to compare the structural responses under the different (classic and adaptive) lateral resistance pressures; No.3 and No.4 were adopted to examine the working performance of the lining structure in the staggered-jointed assembling state during the construction and service periods; the loading conditions from No.5 to No.7 were employed to investigate the sensitivity of structural response to the coefficient of the subgrade reactions, and the sensitivity of structural response to the longitudinal thrusts was studied in loading scheme No.8 to No.11; the ultimate condition (No.12) would give the limit of the inner water head which would be informative for the design optimization. In the single-ring tests, only the loading schemes No.1, 3, 4 and 12 were considered.

Table 1 Loading conditions

No.	Loading condition	Resistance pressure type	Thrust force	Coefficient of subgrade reaction
1	Designed condition	Classic	1000 kN	9000 kPa/m
2	Designed condition	Adaptive	1000 kN	9000 kPa/m
3	Cyclic loading condition	Adaptive	1000 kN	9000 kPa/m
4	Grouting condition	——	1000 kN	——
5	Sensitive analysis on the coefficient of the subgrade reactions	Adaptive	1000 kN	6000 kPa/m
6		Adaptive	1000 kN	9000 kPa/m
7		Adaptive	1000 kN	12000 kPa/m
8	Sensitive analysis on the longitudinal thrusts	Adaptive	300 kN	9000 kPa/m
9		Adaptive	450 kN	9000 kPa/m
10		Adaptive	600 kN	9000 kPa/m
11		Adaptive	1000 kN →0 kN	——
12	Ultimate condition	Classic	0kN	9000 kPa/m

4.3 Measurement program

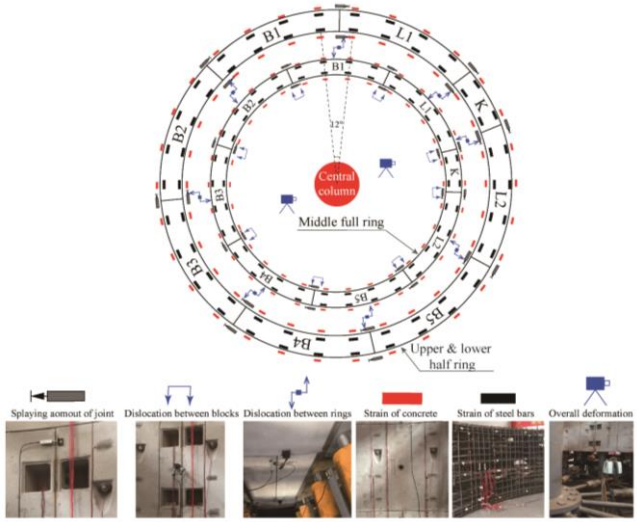

Figure 9 Layout of the routine instrumenttation

The monitoring methods adopted in both two kinds of loading tests were the same. Several contents were monitored to reflect the mechanical responses and the damage mode of the lining systems during the loading tests, including (a)overall deformation; (b)strain of the concrete and rebars; (c)strain of the bolts; (d)opening and closure amounts of the circumferential joints; (e)dislocations between adjacent segmental blocks in both two tests and between adjacent rings in three-ring tests; (f)concrete cracks. The monitoring program in the three-ring tests was given in Table 2, and the layout of the routine monitoring instrumentation was shown in Figure 9.

In additional to the conventional monitoring techniques, two kinds of non-contacting methods were adopted including the 3D laser scanning (see Figure 10a) and DIC-3D image acquisition (see Figure 10b) to measure the convergence deformation of lining ring and cracking process, respectively. Due to the existence of the middle central column, two laser scanners had to be used whose point clouds were merged to form a complete inner outline of the lining system. The detailed data processing method could be referred to Zhang et al. (2019). The inner surface of the lining crown where the minimum axial force and maximum bending moment were present would be the place where the cracks emerged firstly. Therefore, a set of DIC-3D device was fixed in front of the measured zone at the crown to realize the crack visualization. The detailed data processing method could be referred to Zhu et al. (2017).

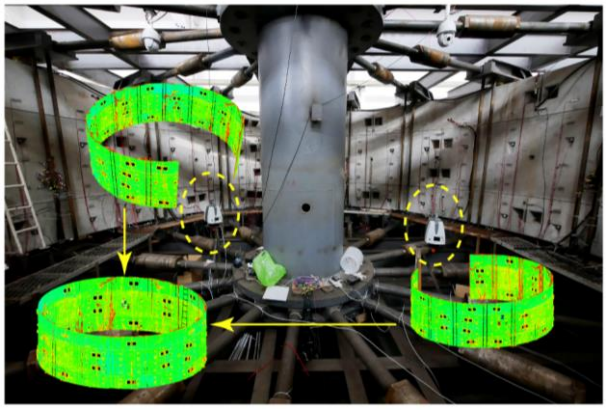

(a)3D laser scanning technique

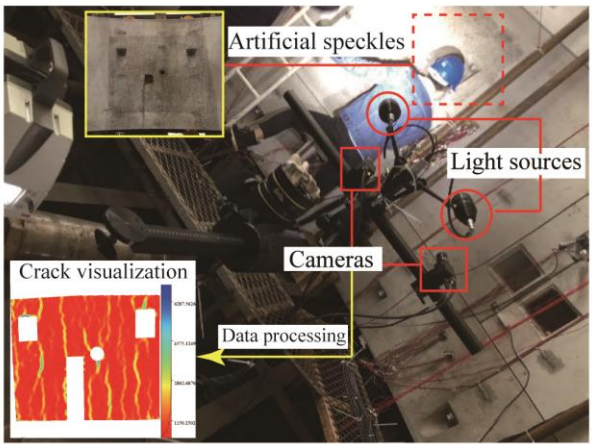

(b) DIC-3d image acquisition device

Figure 10 Special techniques on the capturing the deformation and concrete cracks

Table 2 List of monitoring contents and instrumentation in three-ring tests

Items	Instruments	Range/Accuracy	Quantities
Joint deformation	ZS1100-DT40 displacement transducers	40 mm/0.01 mm	64
Ring-ring/Block-block dislocation	ZS1100-DT40 displacement transducers	40 mm/0.01 mm	32/8
Concrete strain	BX120-50AA foil strain gauges	20000 με/0.01 με	480
Reinforcement/Bolt strain	BX120-5AA foil strain gauges	20000 με/0.01 με	480/128
Overal deformation	3D laser scanners	——	2
Crack width	DIC-3D 3D DIC photogrammetry technique	——	1

5 Testing results

5.1 Mechanical responses in the designed state

5.1.1 Distribution of bending moments

Figure 11 shows the comparisons of the bending moments over the cross-section of the full ring between the single-ring tests and three-ring tests in the ET and UST states. The distribution patterns are similar between different loading tests. More specifically, the lining crown and the invert experienced the maximum positive bending moment, while the maximum negative bending moment was located at the left waist. The negative bending moments of the right waist were much smaller than that at the left waist due to the existence of the sealing roof block which reduced the local structural rigidity. Four zero bending moments were present approximately at 45° in each quadrant. All sections of the lining structure were in compression.

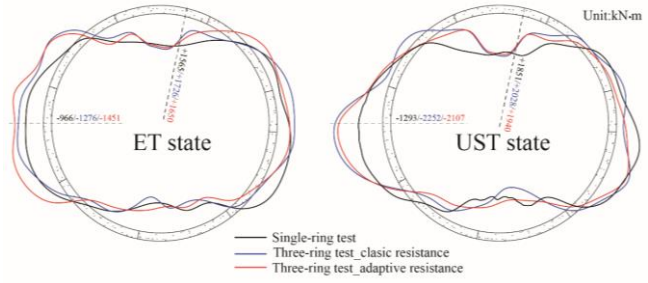

Figure 11 Distribution of the internal forces

Some interesting phenomena can be observed as follows:

- As shown in Figure 12, both the bending moments and axial forces of two characteristic sections were obtained (section 1 in the positive bending moment area, section 2 in the negative bending moment area) to show the influence of the inner water head on the evolution of the internal forces of the segmental body. Through the comparison between the ET state and the states after UST, the increase of the inner water head during the storage significantly reduced the axial forces at almost all sections and only made the bending moment slightly larger;

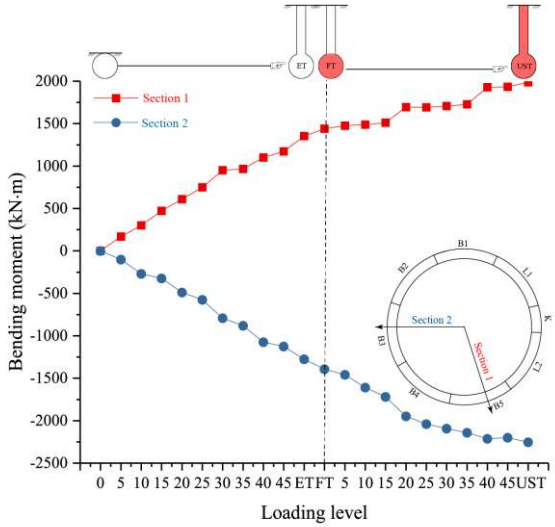

(a) Bending moment

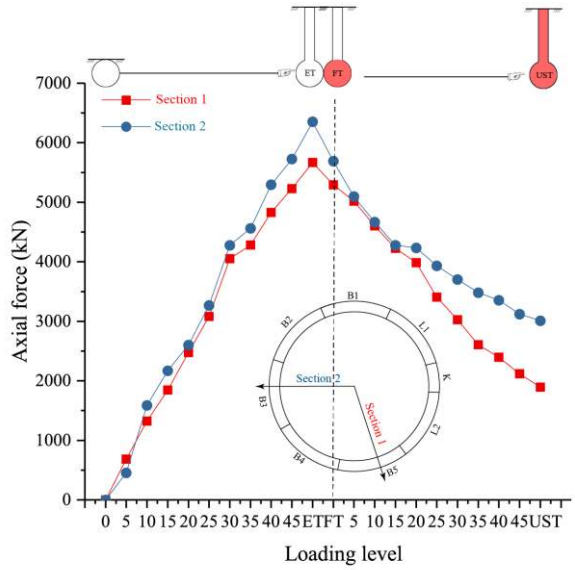

(b) Axial force

Figure 12 Variation of the internal forces with the loading levels

- Compared with the single-ring tests, the shape of bending moment distribution in the three-ring tests was more zigzag, especially at the sections close to the joints as the moment transferring mechanism happened between the joint and the segmental body;
- Compared with the classic theoretical formula of the lateral resistance pressure, the adaptive resistance system which provided real-time reaction forces corresponding to the segmental deformation led to smaller bending moment at both crown and waist areas.

5.1.2 Segmental deformation

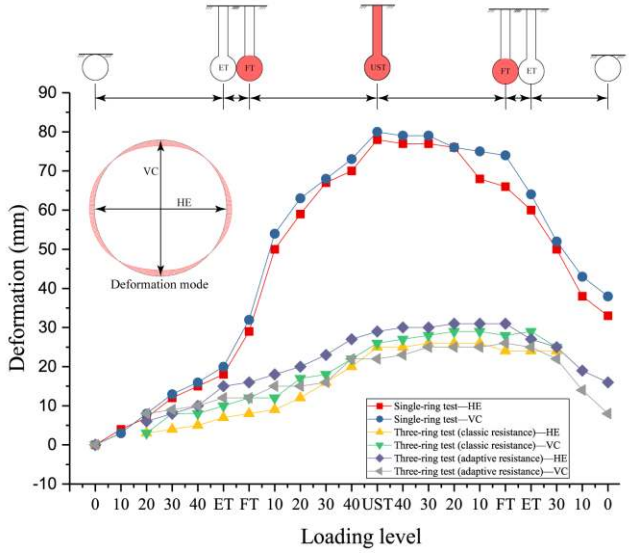

Figure 13 Deformation mode and law with the loading levels

As shown in Figure 13, similar to the traditional deformation mode of circular tunnels, the WSD tunnel of Shanghai also deformed in the pattern of 'expansion in the horizontal direction, and closure in the vertical direction'. Relative displacement between the crown and the invert was named as vertical closure (VC), relative displacement between two twists was named as horizontal expansion (HE). Some common observations can be made by comparing between both two types of loading tests:

- At the stage of increasing burial depth before reaching the ET state, both of the VC and HE increased linearly with the increasing external soil and water pressure, which indicates that the lining structure was overall in an elastic state;
- The structural deformation increased nonlinearly as the inner water head was introduced. The structural deformation developed more rapidly with increasing inner water head than with increasing burial depth. The deformations at the UST stage were much larger than at the ET stage especially in the single-ring tests. Both suggested that the inner water pressure had more notable influence on structural deformation than the external water-soil pressure. This phenomenon was firstly obtained in the water storage and sewage tunnel.
- After the unloading stage, residual deformations still existed owing to the non-elastic characteristic of joints.

However, the structural deformation in the three-ring and single-ring tests also showed several different features:

- Both VC and HE in the single-ring tests increased more rapidly than those in the three-ring tests at the stage of increasing burial depth. The VC and HE values at ET state were 18 mm and 20mm in the single-ring tests compared with the corresponding values of 10 mm and 7 mm in the three-ring tests. The differences in growth rate of VC and HE between the single-ring and three-ring tests became increasingly pronounced during the water storage stage. The VC and HE values at the UST state were 78 mm and 80mm respectively in the single-ring tests, which is about 3 times of those in the three-ring tests in which the VC and HE values are 26 mm and 25 mm respectively;
- At the water drainage stage, the structural deformation recovered immediately as the inner water head was reduced in the single-ring tests. However, the structural deformation in the three-ring tests continued to grow slightly and only started to decrease after the inner water head had been reduced to 20 m. The lag of deformation recovering in the three-ring tests can be mainly attributed to the clamping effect of the upper and bottom half rings, which restricted the reversed deformation of the middle full ring;
- These indicated that comparing with the single-ring structure, the overall rigidity of the three-ring structure was strengthened due to the staggered fabrication. On one hand, the clamping effect provided by the upper and bottom half rings restricted the deformation growth of the middle full ring. On the other hand, the moment transferring mechanism at the joints partially transferred the internal force of the joints to the segment bodies of adjacent rings.

The opening amounts of all joints in the UST state of both single-ring and three-ring tests are inllustrated in Figure 14. In accordance with the traditional distribution law, the joints opened in the inner surface and closed in the outer surface at the lining crown and invert regions where positive bending moments were presented, while the joints experiencing negative bending moments opened in the outer surface and closed in the inner surface in both single-ring and three-ring tests, the largest opening amouts were all located at the outer surface of Joint 7 on the left waist of the lining structure where maximum negative bending moment existed The second largest joint deformations were present at the inner surface of Joint 5 which experienced the largest positive bending moment. The joint deformations in the three-ring tests were only one tenth of their corresponding values in the single-ring tests, which showed again that the staggered fabrication enhanced the overall rigidity and the moment transffering mechanism reduced the inner forces at the joints.

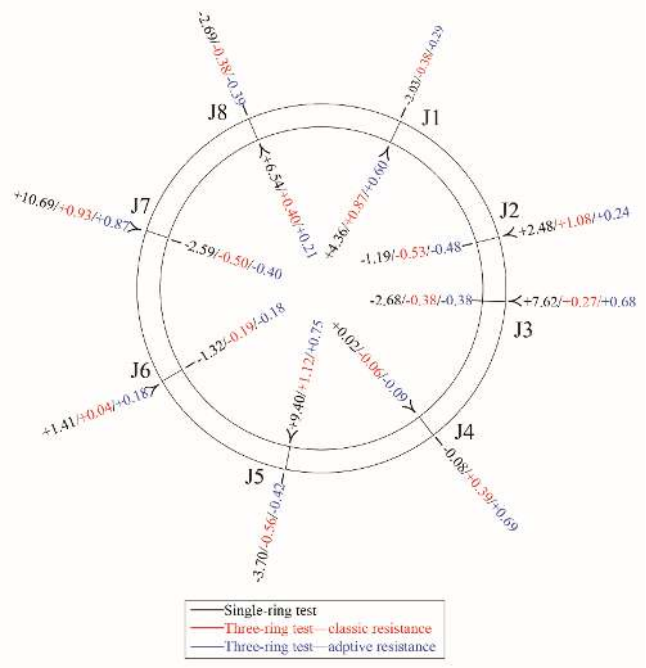

Figure 14 Opening amount of all joints

5.2 Mechanical responses in the cyclic loading condition

Considering that the deformation pattern in the three-ring loading tests was similar to that in the single-ring tests, only the convergence deformations and the bending moments distribution at the two characteristic states, i.e., ET and UST states, are given in Figure 15 and Figure 16 respectively. It should be noted that each loading level was maintained for several minutes until the structural responses became stable during the loading process, and at least 20 minutes must be spent in order to let the lining deform fully once the loads increased to the UST state.

Seen from Figure 15, at the end of the drainage stage in the first cycle (Cycle 1), the convergence deformation caused by water storage did not return to the initial value of ET state because of the non-elastic characteristic of the joints. The deformation law in the subsequent cycles was consistent with Cycle1, but the convergence deformations accumulated slightly after each loading cycle until the tests were stopped.

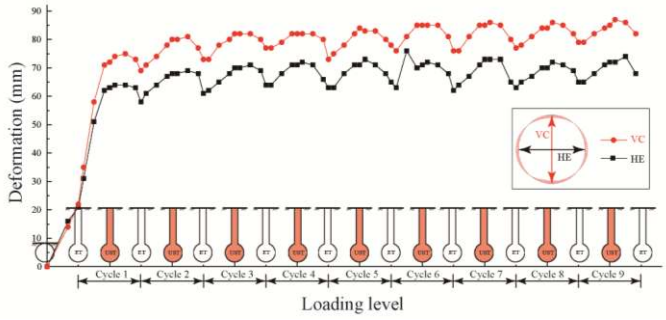

Figure 15 Convergence deformation during the cycle condition

Since the cyclic loading condition lasted for nearly three days, a large number of strain gauges were out of work after continuously working for such a long time, only internal forces at the ET and UST states of the first 6 cycles were given in Figure 16. The bending moments at the same characteristic state were almost identical, which indicated that the current design would be safe and reliable after at least nine loading cycles.

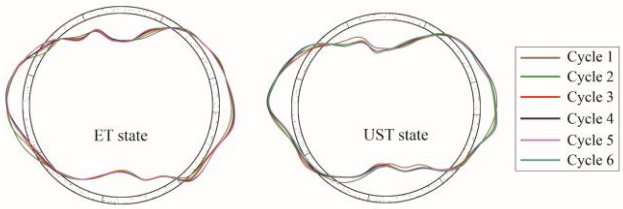

Figure 16 Distribution of the bending moments during the cycle condition

5.3 Mechanical responses in the grouting condition

To keep the force balance of the lining system during the loading process, 6 grouting points distributed symmetrically with respect to the middle central axis were all adopted to simulate the grouting process in the construction period. Through increasing the hydraulic jack loading forces where the grouting points located from 0.1-fold increment (grouting pressure factor 1.1) of the soil and water force to 0.7-fold (grouting pressure factor 1.7), the bearing state when the lining structure was subjected to the grouting pressures in the ET state was finally simulated and the progressive mechanical responses with the grouting pressure factors in the three-ring tests were obtained in Figure 17.

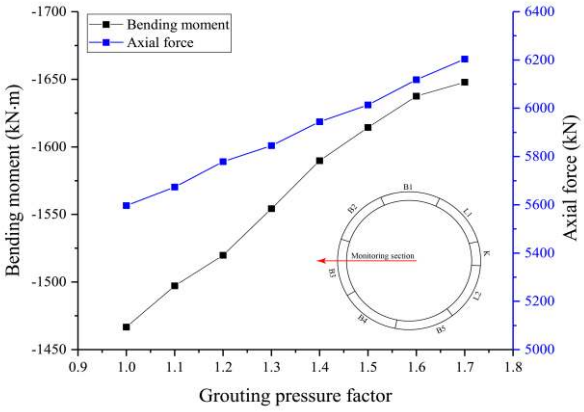

(a) Internal forces

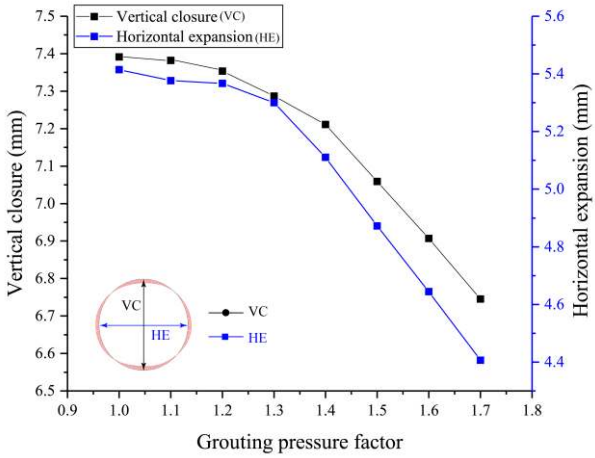

(b)Deformation

Figure 17 Variations of the internal forces and deformation with the grouting pressure factors

Figure 17a shows the evolution of the internal forces with the grouting pressure factors in the left waist, and both the bending moment and axial forces increased linearly owing to the axisymmetric loading method which was approximately equivalent to uniformly applied axial force. The variation of the segmental

deformations with the grouting pressure factors is given in Figure 17b, and both two convergence values decreased as the hoop effect caused by the grouting pressures led to the recovery of the segmental deformations.

No local crushing and large dislocations between the blocks and the rings were observed in the test, and the whole lining system was in a safe state.

5.4 Sensitive analysis of the longitudinal thrusts

To investigate the sensitivity of structural deformation to the longitudinal thrusts, an initial thrust of 1000 kN was applied and the external soil-water pressures gradually increased to the ET state. After the deformation became stable, the thrust forces at each loading point were gradually reduced to zero. The evolution of structural deformation with respect to the longitudinal thrust is shown in Figure 18. The lining deformation increase slowly at the beginning of decreasing longitudinal thrust, then, it increased more rapidly when the thrust force decreased to 520 kN which corresponded to a total thrust of 7800kN. Therefore, 7800kN was determined to be the critical longitudinal thrusts, beyond which the influence of longitudinal thrusts would be negligible.

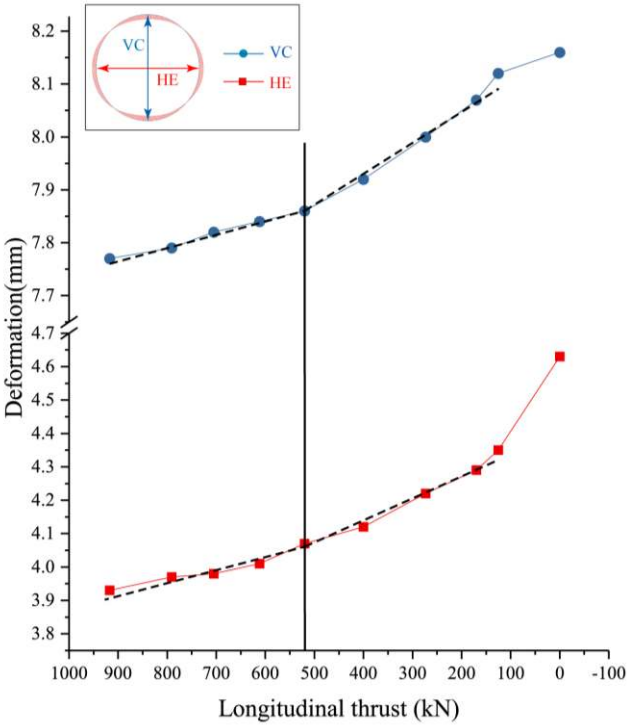

Figure 18 Variations of the deformations with the longitudinal thrusts in the grouting condition

5.5 Sensitive analysis of coefficients of subgrade reaction

The lining structure bears the stratum resistance on both two waists under in-situ stress conditions, as the tunnel deformations are restrained by the surrounding soil, and the magnitude of the coefficient of subgrade reaction determines the stratum resistance to a certain extent. In three-ring tests, adaptive resistance system was employed to investigate the sensitivity of the segmental lining to the coefficients of the subgrade reaction (6000, 9000, 12000,15000kN/m^3), and all four coefficients are available in the soft soil strata of Shanghai.

The variations of the lining deformations with the coefficient of the subgrade reaction were given in Figure 19, and seen from which, the segmental structure was not sensitive enough as the circular tunnel has strong resistance to the deformations and the values are very small during the buried depth increasing stage; in the water storage stage, the sensitivity of the segmental deformations to the coefficients of subgrade reaction became more and more obvious with the increasing of inner water head. Finally, the vertical closures reached 22.5, 21.9, 20.5, 18.9 mm, and the horizontal expansions reached 22.0, 20.6, 19.3, 17.8 mm at the UST state respectively. It could be easily found that both two deformation values decreased linearly with the coefficients of subgrade reaction.

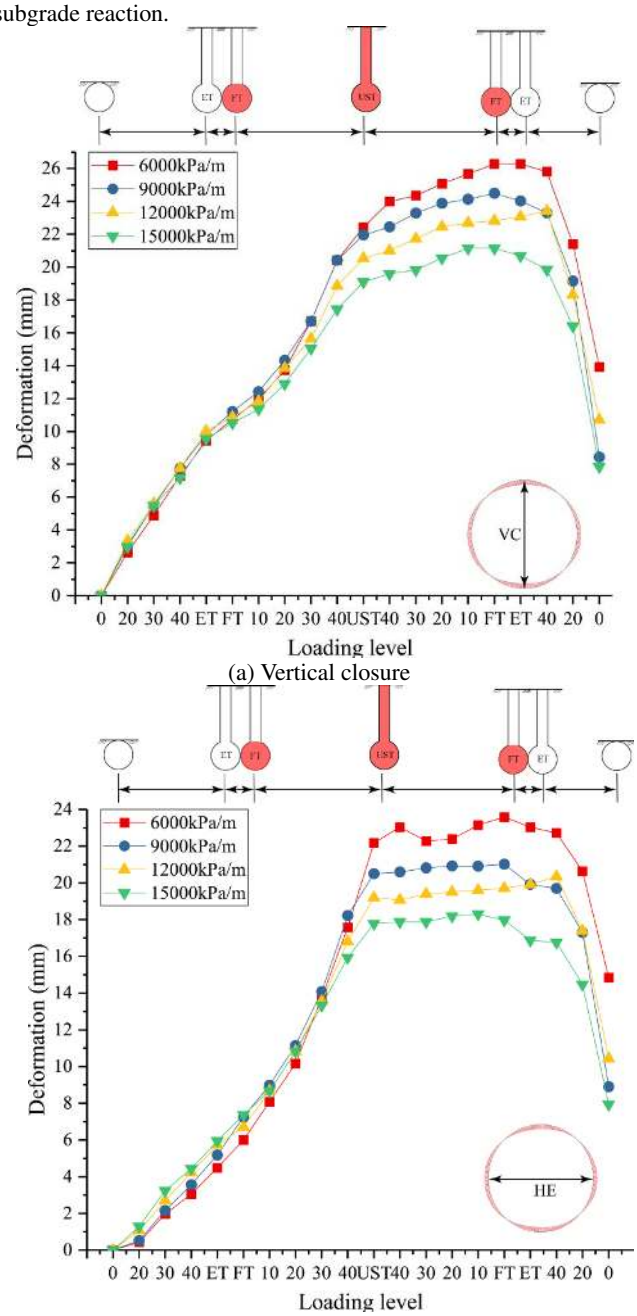

(a) Vertical closure

(b)Horizontal expasion

Figure 19 Variations of the deformations with coefficient of subgrade reaction

5.6 Damage modes

The comparison of the segmental lining deformation between the single-ring and three-ring tests when loaded to the ultimate state are given in Figure 20. As shown in Figure 20a, the variation of the

segmental deformation in the single-ring case can be divided into three stages, and the growth rates increase stage by stage. Especially at the third stage, the deformations experience an exponential growth after the inner water head exceeded 50m, and the whole lining structure was in a plastic deforming state. When the inner water head reached 65m, the intrados of Joint 5 experienced an accelerated opening, while the concrete crushed at the extrados. The test was stopped immediately when four bolts at Joint 5 were pulled off at the same time. At this stage, the vertical closure and horizontal expansions reached 105mm and 117mm, respectively. The phenomenon that the horizontal expansion was larger than vertical convergence deformation may be attributed to the existence of key block at the right waist, which apparently reduced the horizontal rigidity of the lining.

On the contrary, only two linear stages could be figured out in the three-ring tests (see Figure 20b), and the lining structure was still in the elastic state even when the inner water head was 64m. The vertical convergence and horizontal expansion reached 53mm and 51mm, respectively, which were only half of those in the single-ring test. The vertical convergence and horizontal expansion were close to each other, which might be because the reinforcement of adjacent segmental body on the key block made the rigidities of both two waists more symmetric and the stiffness distribution of lining structure more even.

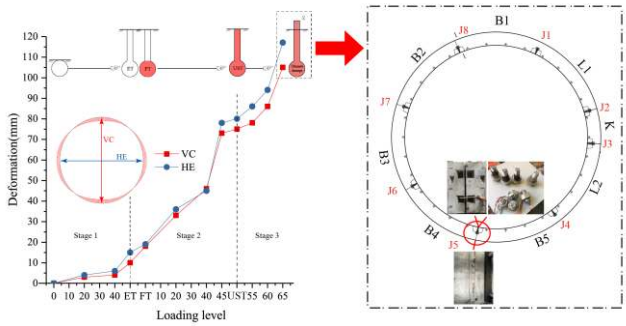

(a) Single-ring test

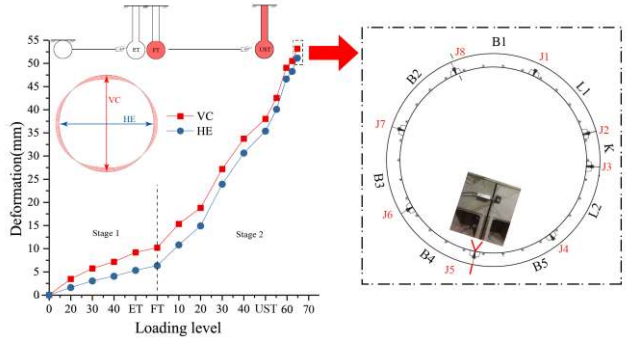

(b)Three-ring test

Figure 20 Variaitons of the deformations for single-ring and three-ring tests

The joint deformation over the cross-section at the ultimate state for both two types of tests are illustrated in Figure 21. Joints still opened at intrados at locations where positive bending moment existed, but the opposite was true at locations in the negative bending moment area. However, the experimental data showed evidently that the joints deformed much smaller (especially in J1, J3, J5 and J7) when the lining structure was in a staggered-jointed fabrication state, which further proves staggered-jointed assembling method makes the lining more stable in the soft soil strata. The tensile stress of the bolt J5 in three-ring test reached 401.7MPa, which approached two-thirds of the bolt tensile strength, and indicated the further bearing capacity of lining.

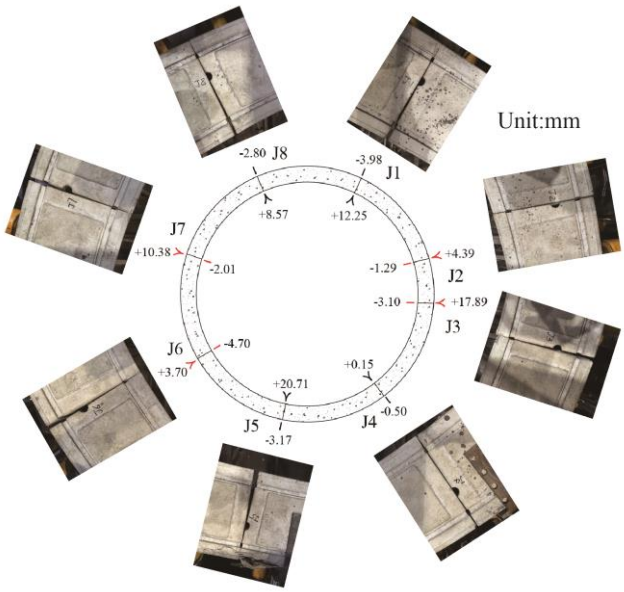

(a) Single-ring test

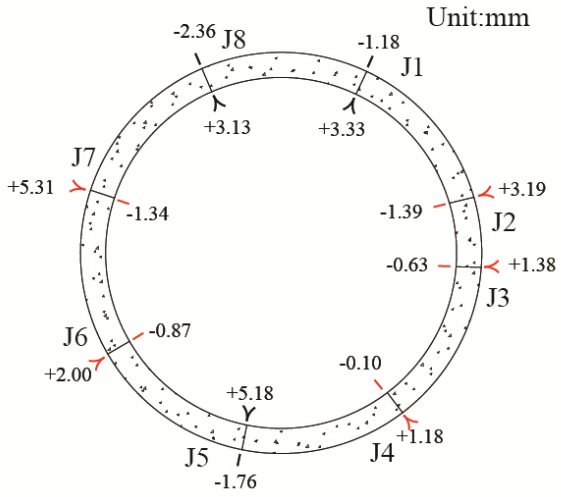

(b)Three-ring test

Figure 21 Joint deformation in the ultimate condition in single-ring tests

The cracks of the full ring from both two tests are sketched in Figure 22 after all segments were uninstalled block by block. The distribution of the cracks follows the distribution of the internal forces in both two types of tests, i.e., the cracks concentrated on the inner surface of the crown and invert and the outer surface of two waists. However, two differences should be underlined between the single-ring tests and three-ring tests:

- Compared with the three-ring tests, the segments deformed more freely at the locations near the key block in the single-ring tests and no cracks were observed at the right waist. The internal forces were transferred to places where the structural stiffness was larger, which led to more obvious cracking phenomenon at intrados of crown and invert as well as at extrados of the left waist;
- Compared with the single-ring tests, the number and propagation length of cracks in each area of the three-ring tests was much smaller as the staggered-fabrication transferred some of the moment from the joints to adjacent lining segment, which increased the overall structural rigidity and the resistance to deformation;

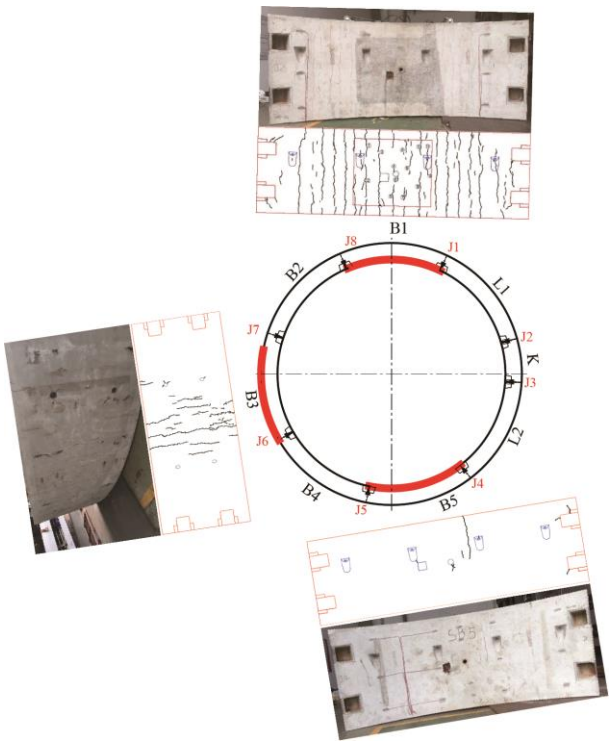

(a) Single-ring test

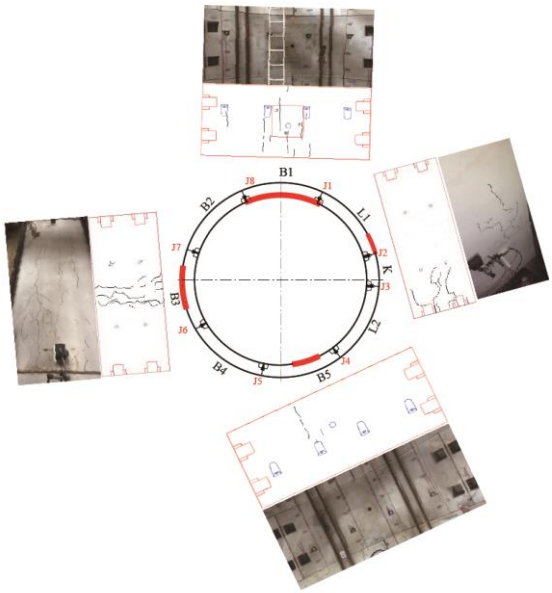

(b) Three-ring test

Figure 22 Distributions of the cracks for both single-ring and three-ring test

As shown in Figure 23, the image process and data analysis revealed that, during the single-ring test, the width of one crack on the inner surface of the lining crown reached 0.2mm with the inner water head of 55m , which is the limit value for the segmental concrete crack prescribed in the Chinese design code (GB50157-2013, 2013). On the contrary, when the tests were stopped at an inner water head of 64m in three-ring tests, the maximum crack width located on the inner surface of the lining crown was only 0.133mm, which indicated that the lining structure was still in a serviceable state.

It should be pointed out that in the single-ring loading tests, the cracks reached the damage standards before the joint bolts were pulled off, which means the lining structure reached the serviceability limit state when the inner water head was 55m, and reached ultimate limit state when the inner water head reached 65m. Both two values provided useful information for design optimization considering exhausting the strength of both concrete and bolts simultaneously.

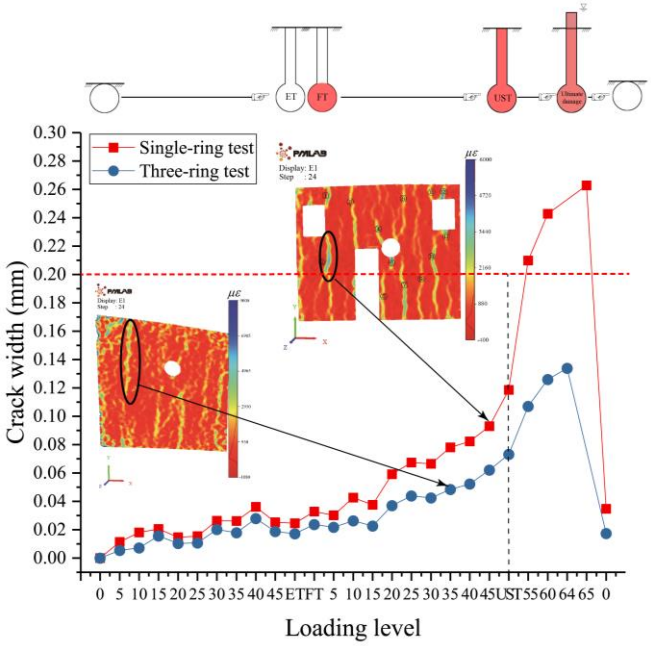

Figure 23 variations of the crack widths for single-ring and three-ring tests

6 Conclusions and suggestions

A series of prototype loading tests including single-ring tests and three-ring tests were performed to investigate the structural responses and deformation laws of the lining structure of a deeply-buried water storage and drainage tunnel. Following observations were made through the comparison between the tests results of single-ring and three-ring loading tests:

(1) The distribution patterns of the internal forces and deformations of the full ring structure were consistent with those reported in the existing researches on circular tunnels. For the first time, it was shown that the increase of inner water head reduced the axial force which leads to obvious increase of overall lining deformation. Furthermore, increasing inner water head had more pronounced influence on the lining deformation than increasing external soil-water pressures.

(2) The staggered fabrication enhanced the integrity of the lining structure and induced obvious bending moment transmission at the joints. Therefore, the overall structural deformation and joint opening amounts obtained in the three-ring tests were much smaller than in the single-ring tests.

(3) The overall structural deformation did not fully recover when the applied loads were unloaded to zero because of the non-elastic characteristic of the segmental joints. During the water inflow and drainage cycles, the inner forces remained approximately unchanged but the residual deformation accumulated bit by bit during the 9 loading cycles. No sudden changes in structural deformation were observed, indicating that the currently-designed lining structure would be still in good performance after 9 water inflow and drainage cycles.

(4) The internal forces increased linearly and the convergence deformations decreased approximately linearly with the grouting pressure factors as the axisymmetric loading method was approximately equivalent to uniformly applied axial force, and the lining system was in a safe state during the grouting process.

(5) The structural deformation increased with decreasing longitudinal thrusts. A threshold value of 7800kN was identified, beyond which, the lining deformation would be less sensitive to the longitudinal thrusts.
(6) Compared with the increasing buried depth, the lining deformations were more sensitive to the coefficients of subgrade reaction when the water inflow into the tunnel, and the deformation values at the UST states decreased linearly with the coefficients.
(7) The lining structure failed when the inner water head reached 65 m in the single-ring tests. The segment body failed prior to the joints. Optimization can be made to fully realize the bearing capacity of joints and segment body.

The paper provides insight for the mechanical behavior of water storage and sewage tunnels and the observations made in the current study can be useful for further optimization of the design of lining structure, as well as construction and maintenance.

7 REFERENCES

Afshan, S., Yu, J. B. Y., Standing, J. R., et al. (2017) "Ultimate capacity of a segmental grey cast iron tunnel lining ring subjected to large deformations". Tunnelling and Underground Space Technology, 64, pp74-84.

Arnau O, and Molins C. (2011) "Experimental and analytical study of the structural response of segmental tunnel linings based on an in situ loading test. Part 2: Numerical simulation". 26, Issue 6, pp778-788.

Bowles, J. E. (1988) Foundation Analysis and Design, McGraw-Hill, New York, pp855-868.

GB50157-2013, Code for Design of Metro. (2013). Beijing: China Architecture and Building Press, pp82-83.

Gragnano, C. G., Fargnoli, V., Amorosi, A., et al. (2015) "3D numerical modelling of soil–structure interaction during EPB tunneling". Géotechnique, 65, Issue 1, pp23-37.

Huang, X., Liu, W., Zhang, Z. X., et al. (2019) "Exploring the three-dimensional response of a water storage and sewage tunnel based on full-scale loading tests". Tunnelling and Underground Space Technology, 88, pp156-168

Huang, X., Zhu, Y. T., Zhang, Z. X., et al. (2018) "Mechanical behaviour of segmental lining of a sub-rectangular shield tunnel under self-weight". Tunnelling and Underground Space Technology, 74, pp131-144.

Lee, K. M., and Ge, X. W. (2001) "The equivalence of a jointed shield-driven tunnel lining to a continuous ring structure". Canadian Geotechnical Journal, 38, Issue 3, pp461-483.

Liu, C., Zhang, Z. X., Regueiro, R. A. (2014) "Pile and pile group response to tunnelling using a large diameter slurry shield – Case study in Shanghai". Computers and Geotechnics, 59, pp21-43.

Liu, X., Bai Y., Yuan, Y., et al. (2016) "Experimental investigation of the ultimate bearing capacity of continuously jointed segmental tunnel linings". Structure and Infrastructure Engineering, 12, Issue 10, pp1-16.

Liu, X., Liu, Z., Ye, Y. H., et al. (2018) "Mechanical behavior of quasi-rectangular segmental tunnel linings: Further insights from full-scale ring tests". Tunnelling and Underground Space Technology, 79, pp304-318.

Molins, C., and Arnau, O. (2011) "Experimental and analytical study of the structural response of segmental tunnel linings based on an in situ, loading test. Part 1: Test configuration and execution". Tunnelling and Underground Space Technology, 26, Issue 6, pp778-788.

Nakamura, H., Kubota, T., Furukawa, M., et al. (2003) "Unified construction of running track tunnel and crossover tunnel for subway by rectangular shape double track cross-section shield machine". Tunnelling and Underground Space Technology, 18, Issue 2, pp253-262.

Selemetas, D., Shirlaw, J. N., Standing, J. R. (2014) "Greenfield ground response to EPBM tunnelling in London Clay". Géotechnique, 64, Issue 7, pp581-583.

Teachavorasinskun, S., and Chub-Uppakarn, T. (2010) "Influence of segmental joints on tunnel lining". Tunnelling and Underground Space Technology, 25, Issue 4, pp490-494.

Zhang, Z. X., Liu, C., Huang, X., et al. (2016) "Three-dimensional finite-element analysis on ground responses during twin-tunnel construction using the URUP method". Tunnelling and Underground Space Technology, 58, pp133-146.

Zhang, Z. X., Zhu, Y. T., Zhu, Y. F., et al. (2017) "Study on the longitudinal mechanical behavior of large shield lining structure with a special-shaped cross-section". Journal of Tongji University (Natural Science),45, Issue 5, pp72-79.

Zhu, Y. T., Zhang, Z. X., Huang, X., et al. (2018) "Prototype Loading Tests on Full-Ring Segmental Lining of Rectangular Shield Tunnel". Journal of Shanghai Jiaotong University (Science), 23, Issue 6, pp 746–757.

Zhang, Z. X., Zhu, Y. T., Huang, X., et al. (2019) " 'Standing' full-scale loading tests on the mechanical behavior of a special-shape shield lining under shallowly-buried conditions". Tunnelling and Underground Space Technology, 86, pp34-50.

Zhu, Y. T., Zhang, Z. X., Zhu, Y. F., et al. (2018) "Capturing the cracking characteristics of concrete lining during prototype tests of a special-shaped tunnel using 3D DIC photogrammetry". European Journal of Environmental and Civil Engineering, 22, Issue sup1, pp179-199.